Gel-induced dew condensation

R. Urbina, S. Lefavrais, L. Royon, A. Mongruel, W. González-Viñas, D. Beysens

GEL-INDUCED DEW CONDENSATION

R. Urbina[1,2], S. Lefavrais[1,3], L. Royon[4], A. Mongruel[1], W. González-Viñas[2], D. Beysens[1,3,*]

[1] Physique et Mécanique des Milieux Hétérogènes, UMR 7636 CNRS, ESPCI Paris - PSL University,
Sorbonne Université, Sorbonne Paris Cité, 75005 Paris, France
[2] Universidad de Navarra, PHYSMED and Complex Systems groups, Pamplona. Spain
[3] OPUR, 2 rue Verderet, 75016 Paris, France
[4] Laboratoire des Énergies de Demain, Sorbonne Paris Cité, UMR 8236CNRS, 75013 Paris, France
* Corresponding author E-mail: daniel.beysens@espci.fr

Keywords
Water Harvesting; Hydrogel; Dew Condensation; Vapor Adsorption

Highlights

- Hydrogels harvest more dew water from atmosphere than regular bare surfaces
- Dew enhancement on hydrogels is due to vapor adsorption adding to condensation

Abstract

Hydrogels are known to adsorb a large amount of vapor and liquid water, making them good candidates to enhance the amount of dew condensed from atmosphere. Although water vapor adsorption and liquid invasion in hydrogels have been the object of many studies, water condensation has been only little investigated. We address here the process of dew

condensation on hydrogel grains widely used in agriculture (Aquasorb 3005^{TM}). We show that dew condensing on hydrogels is enhanced when compared to a regular bare substrate due to vapor adsorption, which adds to condensation. Hydrogels, which can both capture water by vapor adsorption and condense water vapor with high efficiency, are thus good candidates to harvest water vapor from atmosphere with higher yield than regular bare surfaces.

1. Introduction

Hydrogels are three-dimensional networks of hydrophilic polymers, whose properties are known since more than 50 years (see e.g. Wichterle and Lím, 1960). There are many types of hydrogels (e.g. pH-, temperature-, electro- sensitive, light-responsive, etc.), with several applications related to their extraordinary swelling properties (volume can be multiplied by 1000) when immersed in liquid water (for a review, see e.g. Majee, 2016; Ganji et al., 2010). The osmotic pressure attributed to the polymer network is the driving force of swelling. An osmotic gradient indeed forms between the water solvent, low in ionic solute, towards the polymer, rich in ionic solute. The swelling process distends the network and is counterbalanced by the elastic contractility of the stretched polymer network. Due to this osmotic pressure, hydrogels can also exhibit high water adsorption from water vapor (they are hygroscopic), an adsorption which increases with relative humidity *RH* (see e.g. Delavoipière et al., 2018), making them suitable for atmospheric water harvesting (Zhao et al., 2019). Water in hydrogels can be recovered by a moderate (~ 1 bar) osmotic mechanical pressure (Milimouk et al., 2001; Zhang et al., 2017). The osmotic pressure exerted by plant roots in presence of soil water, on the order of 0.1 - 1.2 MPa, can be high enough to extract water from the gel mixed with soil and so provide water to the plant roots (Rudzinski et al., 2002; Puoci et al., 2008). For agriculture in arid and semi-arid environments, there is an obvious

interest to swell the gels with water obtained at the place where they need to be used, thus preventing water transportation on long distances. In consequence, collecting water from humid air by adsorption and/or dew condensation is very appealing.

The question we thus address in this study is whether, once exposed to humid air at night and cooled near or below the dew point, a typical hydrogel used in agriculture (Aquasorb 3005^{TM}) could adsorb and/or condense more water than regular surfaces do. It appears that hydrogel can indeed condense water at a larger rate than a bare substrate. In addition, when gel temperature is above the dew point temperature, water adsorption still occurs.

The paper is organized as follows. After this introduction, details about the experiments and methods are given. Then the water adsorption process is studied for relative humidity lower than 100%, followed by condensation / adsorption proceeding at supersaturation larger than 1. The paper ends by some concluding remarks concerning the main results of the study.

2. Experiments and methods

The absorbent materials are samples of Aquasorb 3005^{TM}, manufactured by SNF Floeger, a granular polyacrylamide. The materials are cross-linked copolymers of acrylamide and potassium acrylate, which are water insoluble and have a very high absorption capacity (ratio water weight/hydrogel weight up to 400). Further information can be found in Table 1 and from Aquasorb 3005^{TM} (2020). The samples can be found in three sizes presentation (Dąbrowska and Lejcuś, 2012): small-size grains (diameter 0.19 ± 0.07 mm), medium-size grains (diameter 0.70 ± 0.2 mm) and large-size grains (diameter 1.5 ± 0.4 mm). Hereby we report results with small and medium grains.

The experimental apparatus is depicted in Fig. 1. It is placed inside a climatic chamber where air temperature and humidity are controlled. The setup consists of a cooling device, a silicon

(Si) plate of diameter 10 cm and thickness 0.7 mm (condensing surface $S_c = 7.853 \times 10^{-3}$ m^2) , which holds the considered sample, and a balance to register the overall weight of sample and Si plate. The cooling device is held by a motorized support which moves it from an upper position, where it is in contact with the plate, to a lower position, where the plate is suspended by holders attached to the electronic balance and can be weighted. The Si plate is usually in contact with the cooling device. Each 38 s, the plate is moved to the lower position to be weighed, a step which lasts about 8 s. Temperature of the cooled plate is measured by calibrated thermocouples with an accuracy of 0.1 °C and a sensitivity of 0.01°C. In the chamber, air temperature T_a is set at 20 ± 0.5 °C and relative humidity at 50 ± 3 %, which corresponds to a vapor pressure of 1.15 kPa and a dew point temperature $T_d = 9.3 \pm 0.1$ °C. The gel sample grains are poured on the silicon plate by the help of a circular mold which keeps the sample height less than 1 mm (small and medium grains) to form a thin layer. In order to have identical departure conditions in all cases, all the samples were previously dried at 40 °C during 8 hours and stored in a closed box with silica gel to maintain a low humidity level. For each experiment, the conditions inside the chamber and the cooling device temperature are fixed at their desired value before placing the plate with the gel.

Two different conditions were investigated, above or below the dew point, which corresponds to either relative humidity $RH \leq 100\%$ (above the dew point) or supersaturation $SR > 1$ (below the dew point). Relative humidity and supersaturation are defined from water vapor pressures as

$$SR \text{ or } RH/100 = \frac{p(T_a)}{p_s(T_p)} \quad (1)$$

Here, $p(T_a)$ is the water vapor pressure in the air surrounding the plate and $p_s(T_p)$ is the water vapor saturation pressure at substrate (plate) temperature. In addition to the

101 determination of characteristic adsorption isotherms under various *RH*, typical temperature
102 conditions as encountered at night outdoors were specially investigated: (i) Above the dew
103 point with a plate temperature $T_p = T_d + 4$ K (adsorption), (ii) below the dew point : $T_p = T_d - 4$
104 K.
105

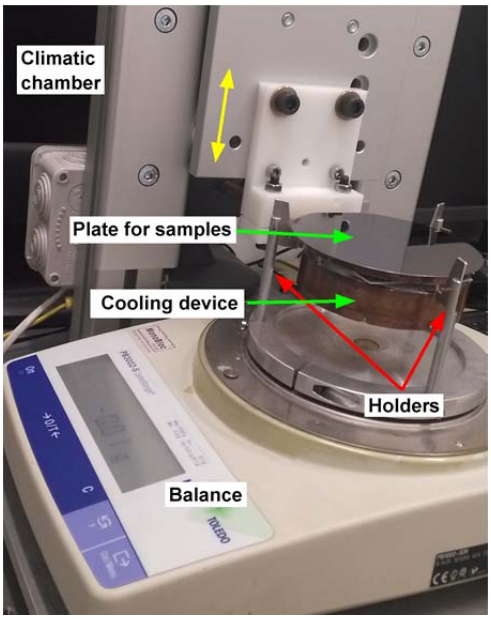

106
107
108 Fig. 1. Experimental setup in the climatic chamber. The sample is placed on a silicon plate
109 cooled from below. The cooling device moves vertically (yellow double arrow). In the upper
110 position, the cooling device is in contact with the plate and controls its temperature. In the
111 lower position, the plate remains suspended from the holders fixed to the balance (red arrows)
112 and the weight can be measured. A thermocouple is fixed below the plate to measure its
113 temperature T_p.
114

Parameters	*small size*	*medium size*
Grain diameter (mm)	0.19 ± 0.07	0.70 ± 0.20
Specific weight (g.cm^{-3})	1.1	
Absorption capacity in 24 h. (water mass/dry gel mass)	336	369

115

Table 1. Some data on Aquasorb 3005^{TM} gel (from Dąbrowska and Lejcuś, 2012 and Aquasorb 3005, 2020).

3. Above the dew point

The dynamics of adsorption is classically governed by two processes (see e.g. Ganji et al., 2010). One process is water molecules diffusing in the gel by Fick's law due to the difference of water concentration between humid air (c_0, corresponding to water vapor pressure $p \sim RH$) and water concentration in gel (c_c). The other process is the stretching relaxation of the polymer chains.

For typical times corresponding to adsorption amplitudes lower than 60% of the limiting saturation value, the adsorption data measured by $\omega_i = m_w/m_i$ (m corresponds to mass with subscript w for water and subscript i = s *or* m for dry small and medium size gel grains) can be fitted to the power law revealing the mode of relaxation:

$$\omega_i = m_w/m_i = A_i t^x \quad (2)$$

A_i is an amplitude and x an exponent whose value corresponds to the gel relaxation process. For pure Fickian diffusion, x = 1/2. For pure gel relaxation, x = 1. In general, the exponent is between 1/2 and 1, corresponding to both relaxation-controlled transport and diffusion-controlled processes. Equation 2 can thus be generalized. With A_i, B_i corresponding to amplitudes related to the two processes:

$$\omega_i = A_i t^{1/2} + B_i t \quad (3)$$

For adsorption amplitudes larger than 60% of the limiting saturation value, the approach to saturation can be described in the case of diffusion by the Fick's law. For a spherical particle of radius R, initial radius R_i and surface $S = 4\pi R^2$ one obtains, neglecting the radius change in the concentration gradient as swelling remains small in the adsorption process:

$$\frac{1}{S}\frac{dm_w}{dt} = -D_p \nabla c = D_p \frac{c_0 - c_c}{R} \sim D_p \frac{c_0 - c_c}{R_i} \quad (4)$$

where D_p is the water diffusion coefficient in the polymer.

The adsorbed mass corresponds to water concentration in the gel, $c_c = 3\, m_w/(4\pi R_i^3)$. The solution to this equation leads to the following exponential decay evolution, in terms of ratio ω_i:

$$\omega_i = \omega_{i,\infty}\left(1 - e^{-t/\tau_i}\right) \quad (5)$$

Here $\omega_{i,\infty}$ is the maximum rate of water in the saturated gel,

$$\omega_{i,\infty} = \frac{4\pi R_i^3 c_0}{3m_i} \propto RH \quad (6)$$

and the typical relaxation time, τ_i, reads as

$$\tau_i = \frac{R_i^2}{3D_p} \quad (7)$$

Since the diffusion of vapor around the grains limits the process (as in the case of thin film studies by Delavoipière et al. (2018)), the adsorption dynamics depends on the thickness of the diffuse boundary layer, that is the layer where a Peclet number $Pe = \frac{UL}{D} < 1$. Here, U is the air flow velocity far from the substrate, L is the characteristic length of the substrate and D is the diffusivity of water molecules in air. In our study, the hydrodynamic conditions are the same for all studied substrates, small or medium grains, and difference in kinetics can be only attributed to *RH* and the grain size.

In the case where the gel relaxation dominates the process, a relation similar to Eq. 5 is found, however with a relaxation time which is independent of gel grain radius and relates to the relaxation of the gel network,

$$\omega_i = \omega'_{i,\infty}\left(1 - e^{-t/\tau'_i}\right) \tag{8}$$

with $\tau'_i = const.$

The evolution due to diffusion plus gel relaxation can thus be written as:

$$\omega_i = \omega_{i,\infty}\left(1 - e^{-t/\tau_i}\right) + \omega'_{i,\infty}\left(1 - e^{-t/\tau'_i}\right) \tag{9}$$

In Fig. 2 are reported typical adsorption isotherms and in Table 2 the results of the fits to Eqs. 2, 3 using data in the range $\omega_i < 0.6\omega_{i,\infty}$. For small grains, the exponent of single power law, Eq. 2, are found in the range [0.58 – 0.79], with mean value 0.69 closer to 0.5 than to 1, showing that vapor diffusion plays the major role in the relaxation process. This is corroborated with double power law fit, Eq. 3, where the amplitude of the $t^{1/2}$ term is about 10 times larger than the t term. For medium grains, the relaxation is too long to obtain data close

to saturation, then the fit to exponential decay Eq. 5 is made over all the data range, which gives an estimation of $\omega_{m,\infty}$. Data are then fitted to power laws in the range $\omega_m < 0.6\omega_{m,\infty}$. The results of the fit to the exponential relaxation, Eq. 5, are reported in Table 2. According to Eq. 5, the relaxation times $\tau_m/\tau_s \approx (R_m/R_s)^2 \approx 13.6$. The measured ratio is smaller, $\tau_m/\tau_s \approx 4.88$, confirming that gel relaxation also matters. Considering only water diffusion in the polymer, one infers $D_p \sim 10^{-11}$ m^2.s^{-1}, a typical value in gels.

Data (Fig. 2a) show, as expected (see e.g. Delavoipière et al., 2018), that *RH* is the only parameter for the adsorption amplitude $\omega_{i,\infty}$ (see the isotherms at $T_a = T_p = T_d + 11$K and $T_d + 4$K with air at same temperature than the substrate and *RH* = 78%). Adsorption where the plate temperature is at a temperature lower than air ($T_p = T_d + 4$K, air at $T_a = 20$ ºC and *RH*= 50%) would correspond to a mean isotherm at *RH* ≈ 64%. Medium grains isotherms (Fig. 2b) correspond to the last case ($T_p = T_d + 4$K, air at $T_a = 20$ºC and *RH* = 50%).

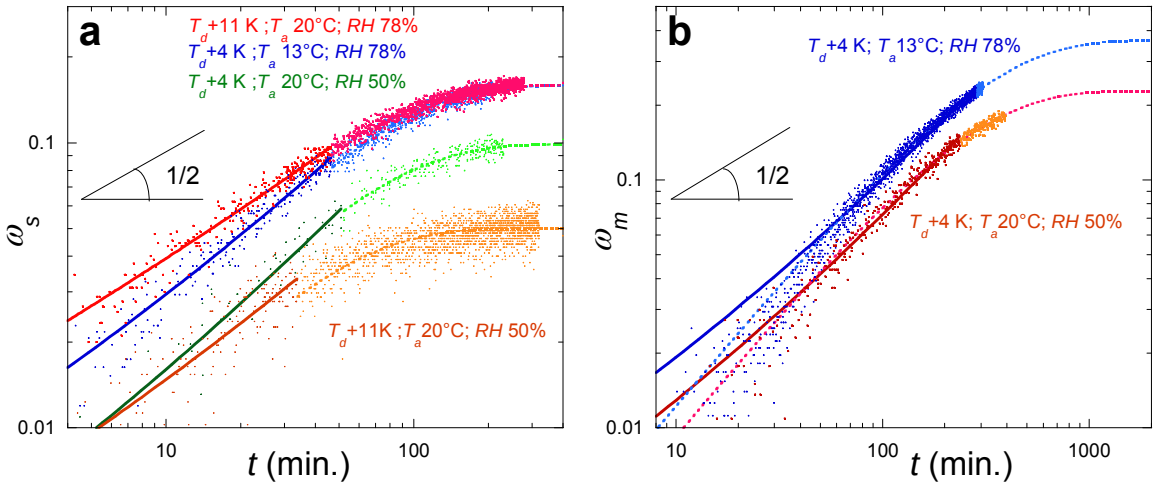

Fig. 2. Evolution of sorption isotherms ($\omega_{i=s,m}$, log-log plot, *RH* < 100%). The full straight lines are power law fits to data 60% below the saturation value (Eq. 2, darker points)) and the interrupted curves are exponential fits to data above 60 % of the saturation value (Eq. 5) (see

206 Table 2). (a) Small grains. (b) Medium grains, where exponential fit is made with all data (see
207 text).
208

Fitting	*Parameter*	*Small grains*				*Medium grains*		*Bare*	
	RH (%)	50	≈ 64	78		≈ 64	78	*SR*	1.32
	T_p-T_d (K)	11	4	4	11	4	4		
	m_i (g)	9.75	9.14	9.20	9.00	7.34	7.14		
Single power law Eq. 2	A_i	0.0032 $\pm 4\times10^{-4}$	0.0026 $\pm 4\times10^{-4}$	0.0056 $\pm 2\times10^{-4}$	0.0102 $\pm 2\times10^{-4}$	0.0169 $\pm 8\times10^{-5}$	0.00257 $\pm 5\times10^{-5}$		
	x	0.66 ± 0.03	0.79 ± 0.04	0.72 ± 0.01	0.58 ± 0.01	0.81 ± 0.03	0.80 ± 0.03		
Double power law Eq. 3	A_i	0.0034 $\pm 4\times10^{-4}$	0.0026 $\pm 6\times10^{-4}$	0.00608 $\pm 3\times10^{-4}$	0.0109 $\pm 2\times10^{-4}$	0.00423 8 $\pm 6\times10^{-6}$	0.0026 $\pm 2\times10^{-4}$		
	B_i	0.00040 $\pm 8\times10^{-5}$	0.0008 $\pm 1\times10^{-4}$	0.00102 $\pm 5\times10^{-5}$	0.0048 $\pm 4\times10^{-5}$	0.00058 6 $\pm 9\times10^{-5}$	0.0004632 4 $\pm 1\times10^{-5}$		
Expo-nential decay Eq. 5	$\omega_{i,\infty}$	0.0499 $\pm 1\times10^{-4}$	0.0989 $\pm 7\times10^{-4}$	0.1593 $\pm 5\times10^{-4}$	0.1592 $\pm 3\times10^{-4}$	0.228 $\pm 2\times10^{-3}$	0.365 $\pm3\times10^{-3}$		
	τ_i (min.)	39 ± 0.6	60 ± 1.5	64.8 ± 0.6	55.8 ± 0.4	242 ± 2	294 ± 3		
Lin. evol. Eq. 11	dh/dt ($\times 10^{-3}$ mm.min.$^{-1}$)							1.4207 $\pm 2\times10^{-3}$	
209
210
211 Table 2. Results of the fits of the adsorption data. Uncertainties: One standard deviation.
212
213 **4. Below the dew point**
214
215 When the substrate temperature is set below the dew point temperature, condensation takes
216 place. Condensation on gels exhibits specific features when compared with condensation on a
217 bare surface.
218
219 *4.1. Region of inhibited condensation.*
220

In Fig. 3 is shown thin (< 1mm) layers of small and medium gel grains in a circle of radius R_g ~ 15 mm on a bare Si surface at $T_p = T_d - 6.7$ K. Dropwise condensation is observed on the Si surface naturally coated with an oxidation layer whose contact angle with water is $\theta \approx 60°$ (see e.g. Narhe et al., 2004).

The hygroscopic nature of the gel due to the osmotic pressure built-up by its hydrophilic sites induces enhanced adsorption of water vapor and thus lowers vapor pressure at the gel border, giving rise to a region of inhibited condensation (RIC) on the bare silicon substrate surrounding the gel sample, with width δ^* as defined in Fig. 3. This RIC is similar to the dry region around lyophilic patches during diethylene glycol condensation (Schafle et al., 2003) or around a salty droplet (Guadarrama-Cetina et al., 2014).

To obtain the δ^* and *Rg* values shown in Fig. 4, the processing of the images includes smoothing, contrast enhancement and border detection, which was performed by using the Fiji® routines. Due to the irregular borders (see Fig. 3), the average distance between the gel and the condensation pattern was determined within a small region.

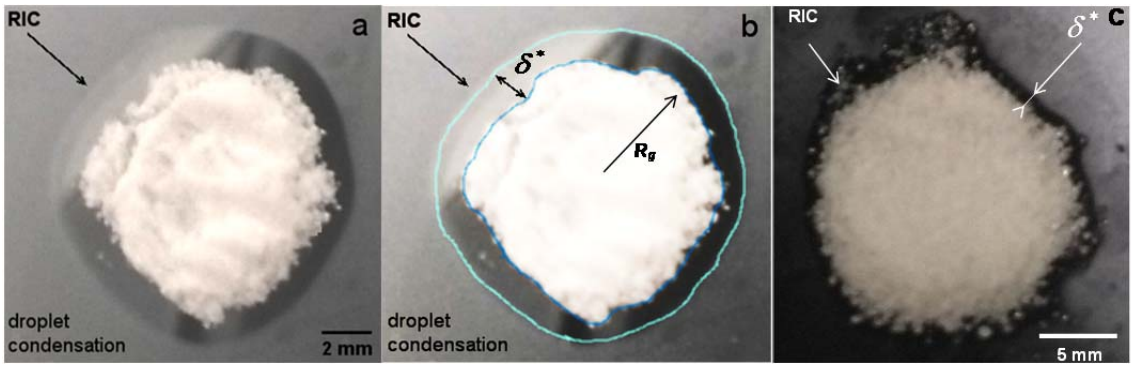

Fig. 3. Examples of region of inhibited condensation (RIC) around a thin (<1 mm) layer of (a, b) small size grain at t = 25 s. (b) is the (a) picture with outlined gel and RIC contours. (c) Medium size grains, t = 25 s. (T_a = 22 °C at 47 % RH, $T_p = T_d - 6.7$ K).

242

243 Figure 4 reports the evolution of the RIC width δ^*, which decreases with time. This RIC
244 decrease can be attributed to the increasing impregnation of the gel with adsorbed water.
245 When the gel is saturated, condensation on gel proceeds with the same way as on the bare
246 substrate, as seen in Section 4.2. The RIC width should be at that time the same as the RIC
247 observed around each water drops or hydrophilic dots (corresponding to the lyophilic patches
248 of Schafle et al., 2003), as a result of the surrounding water vapor gradient (see e.g. Beysens,
249 2018). The mechanism behind the RIC evolution is thus different to what happens with a
250 solute sample (e.g. a salty drop as in Guadarrama-Cetina et al., 2014), which comes from a
251 reduction of saturation pressure (Raoult law) or around an ice crystal where the constant drop
252 in saturation pressure makes the RIC width constant (Nath et al., 2018). (Further analysis is
253 out of the scope of the present study).
254 The evolution of the gel radius increase, $\Delta R_g = R_g(t) - R_g(0)$, is also shown in Fig. 3. The
255 ΔR_g growth rate decreases after about a time ~ 100 s for medium grains, a value near the time
256 where the condensation rate exhibits an inflection corresponding to the lowest influence of the
257 adsorption process (see Fig. 5). The ΔR_g increase is due to both adsorption and condensation
258 processes and is proportional to the collected increasing water volume per unit surface, h ,
259 (see Eq. 11). The prefactor is, however, difficult to precisely evaluate because it depends on
260 the grains packing. It is clear in Fig. 4b that the rate of growth is larger at early times, as in
261 Fig. 5. Note that the ΔR_g behavior can be affected by the grains rearrangement during their
262 swelling, which presumably explains the different behavior between small and medium grains
263 and the oscillations in the R_g evolution as observed in Fig. 4b.
264

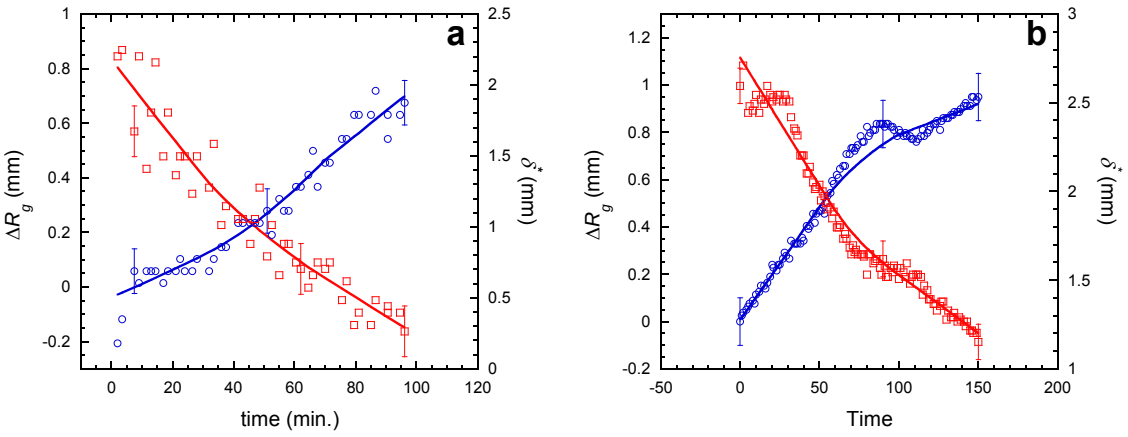

Fig. 4. Evolution of the RIC width δ^* (squares) and gel radius increase ΔR_g (circles) as observed in Fig. 3 of (a) small grains and (b) medium grains. The curves are data smoothing. (T_a = 20 °C, RH= 50%, $T_p = T_d - 4$ K).

4.2. Condensation rates

In order to compare the adsorption volume with respect to condensation on a bare substrate, one considers the surfacic adsorbed volume or equivalent water film thickness, h. With ρ the water density, this layer is expected to grow proportionally to time as

$$h = \frac{m_w}{\rho S_c} \sim t \qquad (11)$$

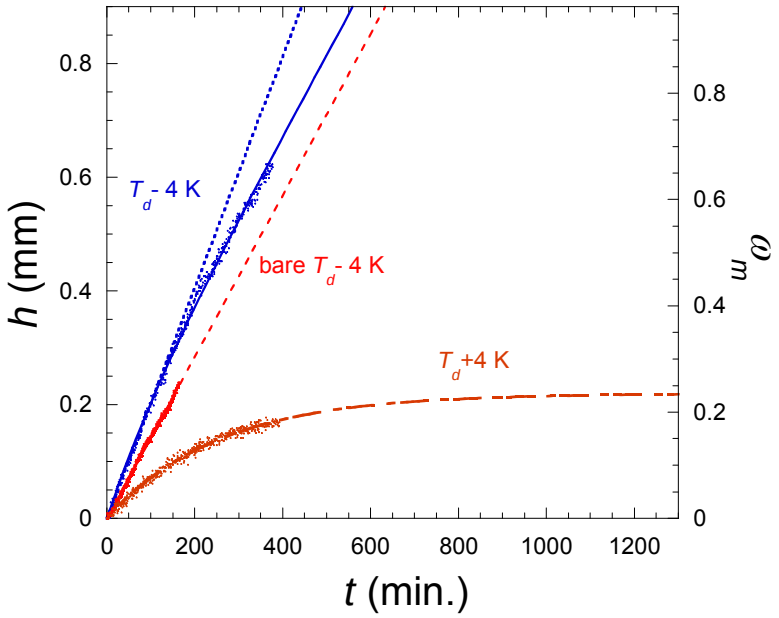

278

279

280 Fig. 5. Evolution of condensation (SR = 1.32) on gel medium grains (blue dots) and bare
281 substrate (red dots) under same conditions (T_a = 20 ºC, RH = 50 %, $T_p = T_d$ - 4 K). Left
282 ordinate: water volume per unit projected area, h. The continuous curve is a fit of gel data to
283 Eq. 12 and the interrupted line is a fit of bare substrate to Eq. 11. The dotted line is the initial
284 slope for condensation on gel. For the sake of comparison, the sorption isotherm at T_a = 20
285 ºC, RH = 50 %, $T_p = T_d$ + 4 K is also reported (orange dots; right ordinate; see Fig. 2b).

286

287 In Fig. 5 is reported condensation on gels and bare substrate. The bare substrate condensation
288 is proportional to time with slope $(dh/dt)_b = 1.4207 \times 10^{-3} \pm 2 \times 10^{-6}$ mm·min^{-1} (uncertainty:
289 1 SD). Gel exhibits a larger initial rate up to time ≈ 100 min. where the rate progressively
290 decreases to reach the bare substrate value, corresponding to condensation and imbibition of
291 the gel as if it were a bare substrate. The swelling ratio at which this inflection occurs (~ 0.2)
292 is far less than the maximum swelling ratio of ~ 370 and cannot be attributed to the vicinity of
293 this limit. One notes that further to this inflection the slope becomes comparable to what is
294 found on the bare surface. This rate decrease towards the bare substrate value can be related to

295 the corresponding decrease of the RIC width and decrease of the rate of gel radius growth,
296 ΔR_g, which occurs during the same time period, and which corresponds to the approach of the
297 saturation of adsorption. In order to assess this point, the gel data have been fitted to the sum
298 of condensation as if the gel were a bare substrate, Eq. 11 and the adsorption evolution, in
299 volume per unit surface as in Eq. 11:
300
301 $$h = \left(\frac{dh}{dt}\right)_b t + h_{m,\infty}\left(1 - e^{-t/\tau_m}\right) \quad (12)$$
302
303 From Table 2, the amplitude value of the adsorption data at T_d + 4K can be expressed in
304 volume per projected gel surface area, $h_{m,\infty} = \omega_{i,\infty} m_i / S_c$ = (0.201 ± 0.002) mm. Figure 5
305 reports the condensation data on gel and bare substrate at T_d − 4K and the adsorption data at
306 T_d + 4K. Gel condensation data are fitted to Eq. 12 with $(dh/dt)_b$ free and imposed. The results
307 are listed in Table 3. When all parameters are left free, $(dh/dt)_b$ is found somewhat smaller
308 than on the bare substrate, presumably because of the lack of data at very long times. The
309 adsorption time is found somewhat lower (195 s) that at T_d + 4K (300 s). The amplitude (0.24
310 mm) compares relatively well with what is expected (0.207 mm). With $(dh/dt)_b$ imposed, the
311 typical adsorption time is 3 time smaller than expected and the adsorption amplitude is too
312 small (0.106 mm). When the adsorption time is fixed at the value at T_d + 4K (≈ 300 s), the
313 amplitude (0.165 mm) increases but still remains smaller than the value at T_d + 4K. With the
314 latter amplitude imposed at 0.207 mm the adsorption time (391 s) becomes closer to the time
315 at T_d + 4K (300 s), with however a χ^2 somewhat larger than the two previous fits. (A more
316 detailed analysis would need more data and is out of the scope of the present study).
317

χ^2 \ Parameters	$(dh/dt)_b$ *(mm.min.$^{-1}$)*	$h_{m,\infty}$ *(mm)*	τ_m *(min.)*
0.070	$(1.1 \pm 0.1) \times 10^{-3}$	0.24 ± 0.05	195 ± 31
0.054	(1.4207×10^{-3})	0.106 ± 0.001	115 ± 4
0.082	(1.4207×10^{-3})	0.165 ± 0.001	(300)
0.15	(1.4207×10^{-3})	(0.201)	391 ± 5

Table 3. Results of the fit to Eq. 11 of condensation data on gel (Fig. 5). The values under brackets are imposed in the fit. The gel mass is m_m = 6.94 g. Notations: see text.

It thus results a net increase of water absorbed on gel when compared to the bare substrate under same conditions, with value on the order of 0.1 mm. This behavior can be explained by the fact that two phenomena are present: (i) an initial adsorption of water vapor, giving a vapor concentration gradient above the surface of the gel larger than on the bare substrate, at the origin of a RIC, followed by (ii) a steady condensation with the same concentration gradient as found above the water drops on the bare substrate. Water will continue to condense on the gel until it reaches its maximum swelling. As a result of the initial large water absorption rate, water absorbed by the gel is thus found in greater amount than water condensed on the bare plate.

Note that if instead of gel particles, one considers a gel film, one should obtain similar enhancement as the adsorption phenomenon is not due to the macroscopic shape of the gel but to the intrinsic properties of the polymer network. A gel film will then equally serve to condense water vapor and the swelling mechanism due to adsorption plus condensation will be the same. The only difference would be the value of the exposed area to condensation, which is smaller, then the condensation rate will be lower. The maximum swelling volume capacity, proportional to the gel volume, will also be smaller. As a matter of fact, such gel film condensation has already been reported by Delavoipière et al., 2018. On the other hand,

340 if there were any non-water vapor absorbing hydrophilic powder on the surface instead of the
341 gel particles, one would simply expect no adsorption. Only filmwise condensation will occur
342 (coefficient $h_{m,\infty} = 0$ in Eq. 12).

343

344 **5. Concluding Remarks**

345

346 Common hydrogels grains used for soil in agriculture (Aquasorb 3005^{TM}) can collect water
347 even for relative humidity less than 100%. They also exhibit interesting properties when used
348 in supersaturation conditions (conditions of dew formation) since they collect more water than
349 a bare hydrophobic substrate with same projected surface area. The measured gain is on order
350 0.1 mm of water / day, which is an important gain when compared to the current values found
351 for dew yield (0.1 - 0.6 mm/day). This enhanced condensation of water is due to the initial
352 water vapor adsorption, which adds to condensation. As noted in the introduction, such
353 condensed water stored in gels can be either used in agriculture where the osmotic pressure
354 exerted by the roots is sufficiently high to extract water or removed by moderate (~ 1 bar)
355 mechanical pressure for human use (Milimouk et al., 2001). Another way is to evaporate
356 water and condense it in e.g. a solar still (see e.g. Zhao et al., 2019 where details on needed
357 energy and time duration are given). Although the use is one and only in agriculture where the
358 grains are definitely mixed with the soil, water extraction by pressure or evaporation has to be
359 cyclically repeated. There is, however, a possible limitation to the number of cycles due to the
360 absorption of CO_2 gas from the atmosphere. HCO_3^- ions are indeed added in the solutions,
361 screening the polymer charges and thus progressively reducing the swelling amplitude (see
362 e.g. Rička and Tanaka,1984 for ions influence). Precise evaluations remain to be carried out.

363 In addition, although the above study has been performed in laboratory by contact cooling,
364 preliminary experiments under outdoor radiative cooling (Beysens, 1998) give, at least

qualitatively, the same results. Emissivity of dry gels is indeed high, as in any organic materials and, when wet, their emissivity becomes close to pure water emissivity (0.98; Schott et al., 2001). Outdoor radiative condensation unsurprisingly exhibits the same properties and constraints than condensation on a solid substrate (e.g. clear sky, high nocturnal relative humidity, low wind speed, water evaporation under direct sun light; see Beysens, 2018). Further research will be needed to get a Proof of Concept, but these results are already very encouraging in view of the development of new materials to enhance dew water collection.

Acknowledgments

We gratefully thank E. Verneuil for discussions. R.U. acknowledges a financial support from the "Asociación de Amigos de la Universidad de Navarra". This work was partially supported by the Spanish AEI (Grants FIS2014-54101-P and FIS2017-83401-P).

References

Aquasorb™ 3005, 2020. https://snf.com.au/downloads/Aquasorb_E.pdf.

Beysens, D., 1998. Outdoor water adsorption and condensation on a polyelectolyte gel. CEA Internal report.

Beysens, D., 2018. Dew Water. Rivers Publisher, Gistrup.

Dąbrowska, J., Lejcuś, K., 2012. Characteristics of selected properties of superabsorbents. Polska Akademia Nauk 3/IV, 59–68. (In Polish).

386 Delavoipière, J., Heurtefeu, B., Teisseire, J., Chateauminois, A., Tran, Y., Fermigier, M.,
387 Verneuil, E., 2018. Swelling Dynamics of Surface-Attached Hydrogel Thin Films in Vapor
388 Flows. Langmuir 34, 15238−15244.

389 Ganji, F., Vasheghani-Farahani, S., Vasheghani-Faraahani, E., 2010. Theoretical Description
390 of Hydrogel Swelling: A Review. Iranian Polymer Journal (English) 5, 375 - 398.

391 Guadarrama-Cetina, J., Narhe, R.D., Beysens D.A., González-Viñas, W. 2014. Droplet
392 pattern and condensation gradient around a humidity sink. Phys. Rev. E 89, 012402

393 Majee, S.B., (Ed.), 2016. Emerging concepts in analysis and applications of hydrogels (
394 Intech, Rijeka).

395 Milimouk, I., Hecht, A.M., Beysens, D., Geissler, E., 2000. Swelling of neutralized
396 polyelectrolyte gels. Polymer 42, 487-494.

397 Narhe, R.D., Beysens, D.A., 2004, Nucleation and growth on a superhydrophobic grooved
398 surface. Phys. Rev. Lett. 93, 076103

399 Nath, S., Bisbano, C.E., Yue, P., Boreyko, J.B., 2018. Duelling dry zones around hygroscopic
400 droplets. J. Fluid Mech. 853, 601-620.

401 Puoci, F., Iemma, F. Spizzirri, U.G., Cirillo, G., Curcio, M, Picci, N., 2008. Polymer in
402 Agriculture: A Review. American Journal of Agricultural and Biological Sciences 3, 299-314.

403 Rudzinski, W.E., Dave, A.M., Vaishnav, U.H., Kumbar, S.G., Kulkarni, A.R. Aminabhavi,
404 T.M. 2002. Hydrogels as controlled release devices in agriculture: Review. Designed
405 Monomers and Polymers 5, 39-65.

406 Schäfle, C., Leiderer, P., Bechinger, C., 2003. Subpattern formation during condensation
407 processes on structured substrates. Europhys. Lett., 63, 394-400.

Schott, J.R., Barsi, J.A., Nordgren, B.L., Raqueño, N.G., de Alwis, D., 2001. Calibration of Landsat thermal data and application to water resource studies. Remote Sensing of Environment 78, 108–117.

Wichterle, O., Lím, D., 1960. Hydrophilic Gels for Biological Use. Nature 185, 117–118.

Zhang Y.R., Tang, L.Q., Xie, B.X., Xu, K.J., Liu, Z.J., Liu, Y.P., Jiang, Z.Y., Dong, S.B., 2017. A Variable Mass Meso-Model for the Mechanical and Water-Expelled Behaviors of PVA Hydrogel in Compression. International Journal of Applied Mechanics 9, 1750044.

Zhao, F., Zhou, X., Liu, Y., Shi, Y., Dai, Y., Guihua, Y., 2019. Super Moisture-Absorbent Gels for All-Weather Atmospheric Water Harvesting. Adv. Mater., 31,1806446